JAAS

ROYAL SOCIETY OF CHEMISTRY

PAPER

View Article Online
View Journal | View Issue

Cite this: *J. Anal. At. Spectrom.*, 2020, **35**, 2620

Quantitative fluorine and bromine detection under ambient conditions *via* molecular emission

M. A. Wakil and Zeyad T. Alwahabi *

The fluorine and bromine limits of detection (LoDs), based on emission from CaF and CaBr, using Microwave-assisted Laser Induced Breakdown Spectroscopy (MW-LIBS) have been determined. The molecular emission bands of CaF and CaBr in the spectral range of 605 nm and 627.1 nm are utilised for quantitative fluorine and bromine detection. The optimum gating has been established for CaF, at 603.3 nm and 605 nm, following 1.5 ms long microwave pulses. The MW-LIBS plasma temperature and electron density against laser energy have been demonstrated at constant microwave power coupling to optimise laser energy using Ca I lines. A linear relationship between the CaF signal strength and fluorine concentration, and CaBr signal strength and bromine in cement has been validated. The recorded limits of fluorine and bromine detection were 106 ± 6 μg g^{-1} and 0.2 ± 0.04%, respectively. The results represent an improved detection limit at low laser energy and 4-fold improved detection limit for bromine.

Received 30th April 2020
Accepted 21st August 2020

DOI: 10.1039/d0ja00200c

rsc.li/jaas

1. Introduction

The detection of halogenated elements is important for the process of analysis, and environmental or geological exploration due to their diverse usage and adverse impacts on the environment, for example depletion of the ozone layer. Given the recent trend of increasing the use of recycled products, halogenated compounds appear to be present in these new products. It is therefore important to analyse these elements under field conditions, which are very difficult to replicate in real time applications.

The uses of halogenated elements and more specifically, fluorine and bromine are evident in different industries. For example, fluorine exists in ionic or combined forms with other chemicals in minerals like fluorspar, fluorapatite, cryolite and other compounds.[1] Fluorides released into the environment through volcanoes, power plants and other high temperature processes usually take the form of hydrogen fluoride gas. Fluorine contained in windblown soils normally consists of large particles, which may settle on the ground or is washed out by the rain.[1] Fluorine and its compounds can be found in fire extinguishers, pharmaceuticals, agrochemical products, dental care, polymers, *etc.*[2,3] In addition, fluorine is used as a compound in industries for manufacturing metallic aluminium, ceramics, and ionic superconducting materials[4,5] Meanwhile bromine, the 62nd most abundant element in the earth's crust, is used as a compound to prevent fouling of internal combustion engines, for fire suppression and in flame retardants.[6] Additionally, brominated compounds are present in many ordinary products such as in plastics in television sets, smartphones, insecticides, *etc.*[7] Conversely, the extreme reactivity of fluorine is highly responsible for various forms of corrosion such as pitting corrosion in steel,[8] corrosion of reinforcement materials,[9] and structural material corrosion.[10] F_2 solution can cause stress-related corrosion cracking in commercially pure titanium, which can worsen the oral cavity.[11] However, due to the economic importance and usage of fluorine and bromine, fast and effective quantitative detection is required.

LIBS is considered to be one of the most popular detection techniques due to its fast, direct, real time chemical analysis of any solid sample. Apart from these advantages, it is found to be less sensitive to certain elements (for example, nuclear fuel) having complex structures,[12] low excitation efficiency[13] and high ionization energy[14] such as halogens. The detection limits for halogens using their atomic lines are less than satisfactory for demanding applications because of their high energy-level distributions. The use of a buffer gas as an inert environment was an effective solution. Asimellis *et al.* detected fluorine at F I 685.6 nm for a concentration of 0.03% under a vacuum helium environment.[15] Gonzalez *et al.* reported a detection limit of fluorine (F) of 109 μg g^{-1} under a reduced argon (Ar) and helium (He) atmosphere using the atomic line at F I 685.6 nm.[5] Pavel *et al.* found a 150 ppm detection limit under a low pressure He environment.[3] Meanwhile Quarles *et al.* discovered a 135 ppm detection limit for F I (685.6 nm) under He purged gas.[16] Kratochvíl *et al.* applied double pulse LIBS in a helium environment and reported a 0.47% detection limit at F I 685.6 nm.[17] In their study, Menghan *et al.* observed a bromine (Br) signal at Br I 827.24 nm in an atmospheric environment.[18] Radziemski *et al.* used the vacuum ultra violet region and reported

School of Chemical Engineering and Advanced Materials, The University of Adelaide, SA 5005, Australia. E-mail: zeyad.alwahabi@adelaide.edu.au

a detection limit of Br of 5.6% at a 163.3 nm atomic line.[19] Barbier *et al.* reported that the limits of detection for Br were 3.6% and 0.9% under air and helium atmospheres, respectively. The measurements were performed at Br I 827.24 nm.[20]

Other possible alternatives to increase the sensitivity of LIBS are to use surrogate measurements or molecular emission rather than atomic emission.[21,22] Gaft *et al.* stated in their study that the use of molecular emission is a potential method to improve plasma emission sensitivity for halogens.[4] Alvarez *et al.* showed in their study that the detection limit of F can be improved by a factor of 25 using CaF molecular emission instead of atomic emission.[2] Forni *et al.* detected a fluorine content amounting to approximately 0.4% using CaF molecular bands for the first time on mars.[23] Alvarez *et al.* calculated a detection limit of 49 μg g^{-1} using CaF molecular emission in calcium-free samples.[14] Pavel *et al.* reported a 65 ppm detection limit of fluorine using a CaF band.[3] In another study, Gaft *et al.* used a bromine-containing compound and observed CaBr molecular emissions at 624.4 nm and 627 nm, respectively.[7]

Microwave-assisted laser induced breakdown spectroscopy (MW-LIBS) is found to be one of the best signal enhancing techniques at a relatively low laser energy, and improves the limit of detection (LoD) compared with LIBS. The MW-LIBS technique has been applied over the last decade due to its distinguishable benefits including long plasma lifetimes, larger volume, strong emission intensity, stability over time, and ability to reduce self-absorption.[13,21,24,25] MW-LIBS offers an extended lifetime to the laser induced plasma. This is usually followed by a relatively longer detection gate of ~500 μs. A longer plasma lifetime along with a prolonged detection gate provides some difficulties because the emission from molecules and radicals becomes stronger, blocking a wide spectral range. However, when the process of molecular formation and emission is carefully used, it can help the detection of halogen elements. Our recent paper on chlorine detection using molecular emission is an example.[26] Here, our focus is on the quantitative detection of fluorine and bromine using the MW-LIBS technique through molecular emissions, namely CaF and CaBr at 605 nm and 627.1 nm, respectively.

2. Experimental details

2.1 MW-LIBS methodology

The experimental setup is conventional single pulse laser induced breakdown spectroscopy that incorporates microwave-assisted laser induced breakdown spectroscopy. The setup system contains a 532 nm Nd:YAG second harmonic laser, Quantel (Brilliant B), ~6 ns with a repetition rate of 10 Hz. A fused silica lens with $F = 100$ mm was used to focus the beam onto the sample surface. The laser beam was propagated onto the sample surface at an angle of 15° to the vertical. 10 mJ and 15 mJ laser energies were used to analyse the CaF and CaBr molecular emission bands, respectively. To achieve the ablation from the fresh sample surface for each shot, the sample was placed on a rotating disk with an angular velocity of 7 revolutions per minute. A second continuous-wave laser[27] armed with a camera served to monitor the exact distance between the sample surface and fused silica lens.

The microwave radiation from a water-cooled pulse-microwave system (Seirem) at 2.45 GHz was directed to a 3-stub impedance tuner through a WR340 waveguide and then to a waveguide-to-coaxial adaptor (WR340RN). A quartz window was used to finalise this process. The waveguide-to-coaxial adaptor was connected to a 1 m flexible coaxial cable (50 Ω NN cable) with 0.14 dB @ 2.45 GHz. A semi-rigid cable (RG402/U) was then connected to the end of the coaxial cable. The other end of the semi-rigid cable was attached to a Near Field Applicator (NFA) as shown in ref. 13 and 28. The NFA was located about 1 mm above the sample surface and 0.5 mm horizontally away from the ablation spot. The microwave pulse duration and power were controlled with an analogue signal pulse generator (Aim-TTi). The microwave pulse duration was kept constant at 1.5 ms.

To analyse the plasma emission, a conventional spectrometer with a gated CCD (Andor, Shamrock 500i) equipped with 300, 1200 and 2400 lines per mm diffraction grating was used. For the experiment, 1200 grating was used. The plasma emission from LIBS was collected directly through a perforated parabolic mirror (FL = 152 mm) and then focused by a plano-convex lens (FL = 100 nm), onto the sample by a plano-convex UV fused silica lens. A second lens (FL = 20 mm) was used to couple the emission onto an Achromatic Reflective Coupler (ARC), which is connected to a 7-fibre bundle (Thorlabs, BFL200HS02). The fibre bundle was a round-to-linear bundle, 7 × Ø 200 μm.

2.2 Materials

Portland cement (~40% Ca) was used as a source of calcium and NaF and KBr salts were supplied by Sigma-Aldrich. Several calibration samples, with different F and Br concentrations, were prepared, by wet impregnation from cement and NaF (and KBr) in order to assess linearity in the calibration curves and for detection of F and Br. Different weights of NaF anhydrous powder, ranging from 4 mg to 150 mg, were mixed with distilled water to make a solution. The same amount of cement, namely 4 g, was then added to the each of the solutions to form several concentrations of F (and Br) in cement matrix. Twelve samples were prepared with an increasing order of the F concentration from 452 μg g^{-1} to 16 958 μg g^{-1}. The pastes of all samples were placed in 25 mm diameter circular disks. The disks were dried in a dryer and the same procedure was repeated for Br containing samples with different weights of KBr, ranging from 20 mg to 450 mg.

2.3 Plasma temperature and electron density

Strong calcium lines were considered for plasma temperature measurements as presented in Table 1. The plasma temperature during the experiment was calculated using the Boltzmann plot.[29]

Electron density was calculated using the calcium line (422.67 nm) according to the relation between the full-width-at-

Table 1 Spectroscopic data of calcium (Ca 1)[34]

Wavelength (nm)	A_{ki} (s^{-1})	E_k (eV)	g
364.441	3.55×10^7	5.3	7
422.673	2.18×10^8	2.93251	3
430.253	1.36×10^8	4.77979	7
445.478	8.7×10^7	4.68133	7
458.587	2.29×10^7	5.22854	9

half-maximum (FWHM) of the line $\Delta\lambda_{1/2}$, and electron density, N_e.[30]

The stark width broadening parameter of (0.115671–0.118173) $\times$ 10^{-6} Å.[31]for Ca I at 422.67 nm considered. To understand if the plasma is at local thermodynamic equilibrium (LTE), the McWhirter criterion was calculated using eqn (1).[32] Fig. 1 presents a typical example of a Boltzmann plot (a) and full width half maximum (b) using the Ca I lines.

$$N_e \geq 1.6 \times 10^{12} \Delta E^3 T_e^{\frac{1}{2}} \quad (1)$$

The instrumental broadening was determined to be 0.0321 nm by recoding the Hg line at 253.6 nm. The value of $\Delta\lambda_{1/2}$ was evaluated using a simple equation.[33]

$$\Delta\lambda_{measured} = \Delta\lambda_{actual} + \Delta\lambda_{instrument}$$

3. Results and discussion

3.1 Spectral information

Typical MW-LIBS spectra concerning the molecular emission of CaF and CaBr are presented in Fig. 2 and 3, respectively. Fig. 2(a) presents CaF in the 603.3 nm and 605 nm range, while Fig. 3(a) illustrates the molecular band of CaBr in the 627.1 nm range. There is a strong emission of CaBr in the 624.8 nm range but this band is found to overlap with other molecular emissions, which makes it difficult to distinguish CaBr at 624.8 nm. The molecular spectral range of CaF and CaBr observed in this study is supported by other studies.[4,7] It is seen in Fig. 3(a) that at a low wavelength (below 625 nm), the pure cement signal is larger than the signal for

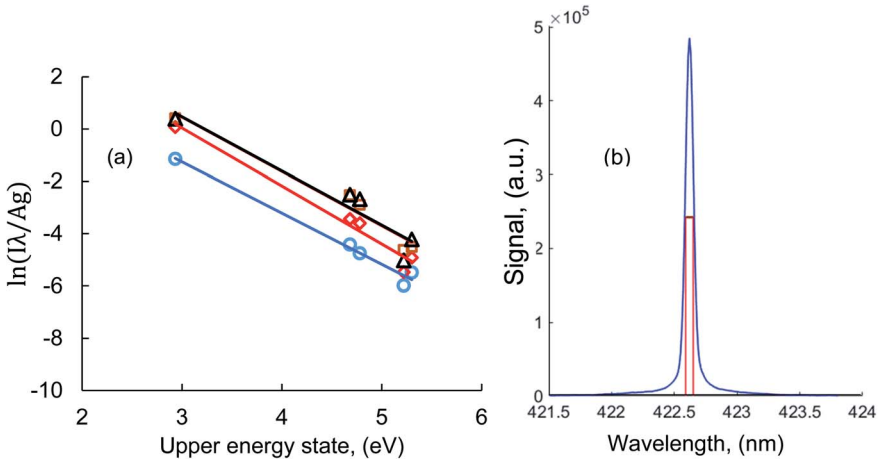

Fig. 1 Boltzmann plot using Ca I lines (a) and a typical example of a full width half-maximum of Ca I at 422.67 nm (b). The experimental conditions were 10 mJ laser energy, 600 W microwave power, 400 ns gate-delay and 300 μs gate-width.

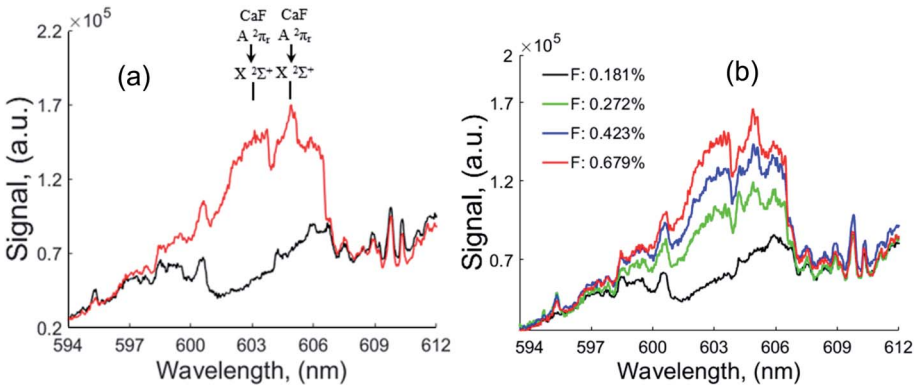

Fig. 2 (a) Typical MW-LIBS spectra of pure Portland cement, black, and Cement+ 0.679% F, red, (b) MW-LIBS spectra for different fluorine concentrations. The spectra recoded at a 10 mJ laser energy, 600 W microwave power, 400 ns gate-delay, 300 μs gate-width and accumulation of 100 shots.

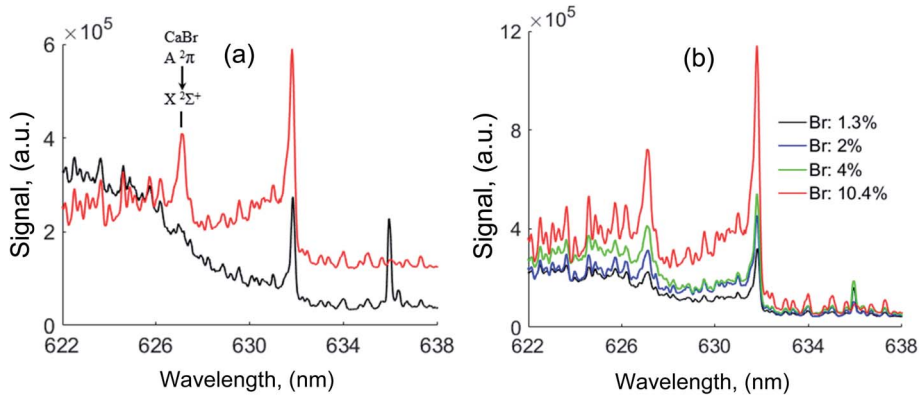

Fig. 3 (a) Typical MW-LIBS spectra of pure Portland cement, black, and Cement+ 10% Br, red, (b) MW-LIBS spectra for different bromine concentrations. The spectra recorded at a 15 mJ laser energy, 750 W microwave power, 400 ns gate-delay, 300 μs gate-width and accumulation of 100 shots.

cement plus 10% bromine. The strong molecular CaO emission around 615 nm was responsible for this which subsequently subsided by addition of bromine in cement. In addition, the strong emission near 631 nm was due to CaCl molecular emission at 631.4 nm.[4] The most intense molecular emission band of CaF lies in the interval between 602.43 and 608.69 and 529.1 nm according to Alvarez *et al.*[2] Gaft *et al.* reported that the strongest molecular CaF bands are in the region of 532.1 nm and 602.9 nm.[4] Furthermore, Gaft *et al.* noted in their other study that the stronger CaBr molecular bands lie in the region of 624.4 nm and 627.0 nm.[7] Bahrini *et al.* asserted in their study that there are molecular CaBr bands in the 377.7 nm, 381.6 nm, 389.4 nm and 393.4 nm regions.[35]

CaF and CaBr molecular formation in the range of 530 nm was not investigated because the wavelength of the ablation laser was 532 nm. An investigation was carried out in the region of 370 nm-398 nm using MW-LIBS but surprisingly, no CaBr molecular emission band was found in this range. The formation of CaF and CaBr molecular spectra depends largely on a calcium-based matrix.[36] Cement was used as a base material for calcium due to the large amount of calcium found in cement (~40% in Portland cement). The spectral ranges 605 nm and 627.1 nm were used to develop the F and Br calibration curves. Fig. 2(b) and 3(b) depict the sample emission spectra of CaF and CaBr for different concentrations of F and Br, respectively, using MW-LIBS. Molecular emission was used in two ranges to obtain the MW-LIBS signal intensity. For CaF and CaBr, the integration of the MW-LIBS signal in the range of (603.32–603.7) nm and (627.04–627.15) nm, was used respectively.

3.2 Effect of laser energy on the signal to noise ratio and plasma parameters

The effect of laser energy with a constant MW power on the MW-LIBS signal was investigated under ambient conditions to optimise the MW-LIBS signal. Fig. 4(a) shows the effect of laser energy on the signal-to-noise ratio (SNR) at a 600 W microwave power. As shown in Fig. 4(a), the SNR above 10 mJ starts to decrease. It was predicted that the microwave's coupling efficiency was the main reason for this result. The increase in laser energy causes electron density in the plasma to increase, which allows the microwave to drive fewer electrons into the plasma and thereby leading to fewer signals. The other reason is the increase in background noise. It has been demonstrated that the SNR can be increased by increasing microwave power.[26] Initially, the microwave cannot be coupled with LIBS plasma due to high electron density in the plasma, but during the

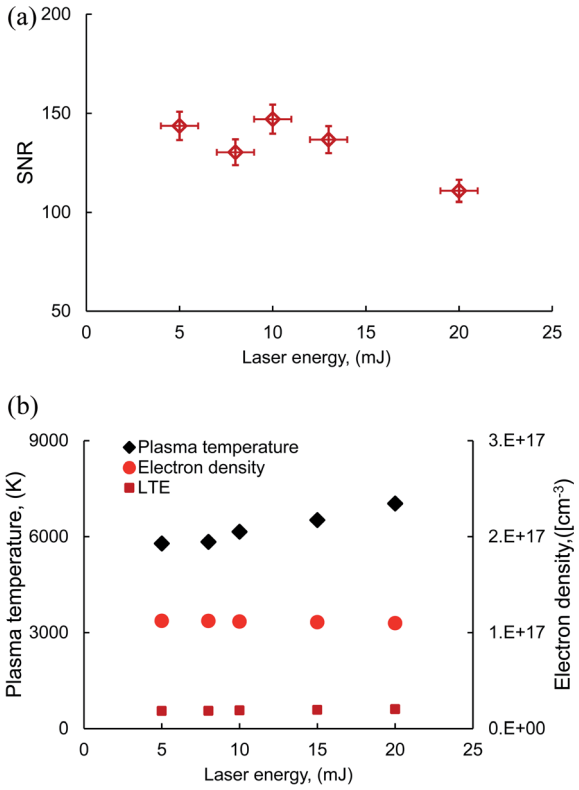

Fig. 4 (a) Signal to noise ratio of molecular CaF at a 600 W microwave power, 400 ns gate-delay, 300 μs gate-width and accumulation of 100 shots. (b) Plasma parameters at a 600 W microwave power, 1 ns gate-delay, and 1 ms gate-width with an accumulation of 100 shots.

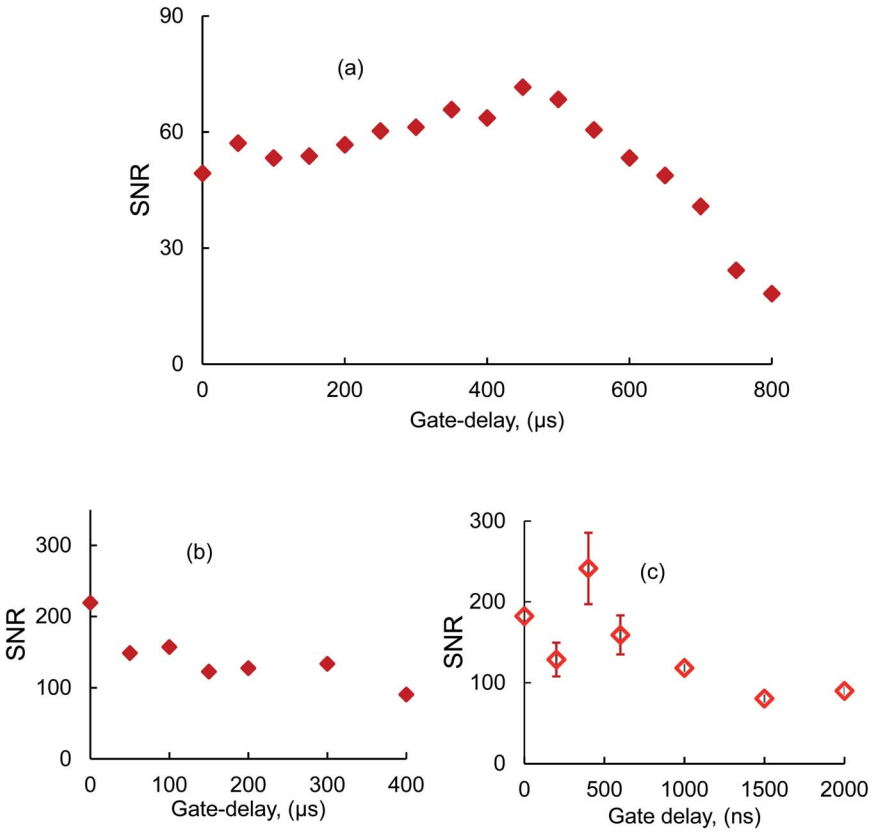

Fig. 5 Temporal evolution (signal to noise ratio) of CaF molecular emission at a 10 mJ laser energy, 600 W microwave power with a (a) 50 μs step and 50 μs gate-width, (b) 0–400 μs gate-delay and 300 μs gate-width and (c) 0–2000 ns gate-delay and 300 μs gate-width.

relaxation of plasma the electron density at the periphery of the plasma falls to below the critical electron density.[37] This allows microwave radiation through the electromagnetic field to drive free electrons and provide them kinetic energy to excite the de-exited atoms and ions by multiple electron-atom or electron-ion collisions.

As long as the microwave remains coupled with the plasma, the emission lifetime improves with longer microwave duration. It has also been demonstrated that the microwave power above 600 W does help to increase the signal significantly but also increases the noise.[26,28,38] For this reason, 600 W microwave power was used in this study. The explanation of the experimental data in Fig. 4(a) is supported by our next experiment as shown in Fig. 4(b). Fig. 4(b) shows the plasma temperature and electron density in the plasma. The plasma temperature and electron density were calculated using the strong Ca I lines as stated previously. It is seen from Fig. 4(b) that the electron density of MW-LIBS is almost constant at fixed microwave power with the increase in laser energy although the plasma temperature increased. This caused a low SNR of MW-LIBS with the increase in laser energy for a constant microwave power because the noise level also increases with the signal. The maximum MW-LIBS plasma temperature was 7036 K, recorded at a laser energy, microwave power and gate-width of 20 mJ, 600 watt and 1 ms respectively. It is worth noting that Khumaeni *et al.* reported a MW-LIBS temperature of 7700 K at a delay-time of 10 μs, measured under reduced-pressure Ar surrounding gas (0.6 kPa).[24]

The calculated electron density, based on MW-LIBS, was found to be much lower than the computed using the eqn (1), as shown in Fig. 4. This is satisfying the Local Thermodynamic Equilibrium (LTE) criteria. For fluorine detection, 10 mJ laser energy was used with 600 W microwave power but for bromine detection, 15 mJ laser energy and 750 W microwave power were employed. The reason for this is due to the CaBr band being relatively weaker than the CaO band that is situated beside the CaBr signal. A slight increase in laser energy caused an increase in the CaBr signal at 750 W microwave power but much higher laser energy was not suitable for optimal CaBr signals. This finding agrees with that of Gaft *et al.*[7]

3.3 Temporal evolution of molecular fluorine

The temporal evolution of molecular CaF emission intensity was investigated and it was found that the gate-delay varied from 0 μs to 800 μs for MW-LIBS. The temporal evolution of MW-LIBS for the CaF signal-to-noise ratio is presented in Fig. 5(a). It is observed from this figure that the SNR of CaF after 500 μs gate-delay started to decrease. Within 500 μs, an experiment was performed maintaining a constant gate-width of 300 μs at a 50 μs gate-delay interval as shown in Fig. 5(b). A 300 μs gate-width was found to be the best for Ca-based molecular emission which is confirmed in another study.[26] As shown in

Fig. 5(b), the SNR of CaF was higher at the earlier gate-delay. In order to examine the optimum gate-delay, the SNR was calculated for 200 ns gate-delay intervals with a constant gate-width of 300 μs as shown in Fig. 5(c). It was observed, that at 400 ns gate-delay the SNR of the CaF molecular emission band emerged as the best. The same outcome was found for CaCl molecular emission as shown in our recently published paper.[26] Gaft *et al.* mentioned in their study that the emission lifetime of CaBr is shorter than that of CaO and the detection of CaBr was better with a short gate-delay.[7] From the experimental data and ESI derived from the literature, 400 ns was considered the ideal gate-delay for F and Br detection using their strongest molecular emissions at 605 nm and 627.1 nm, respectively.

3.4 Quantitative detection of fluorine and bromine

Under optimum experimental conditions of 400 ns gate-delay and 300 μs gate-width, several samples with increasing amounts of fluorine and bromine were analysed to prepare the calibration curves. The temporal conditions were fixed at a 400 ns gate-delay and 300 μs gate-width. Fig. 6 and 7 illustrate the variations in the CaF and CaBr net emission signals *versus* the fluorine and bromine mass content, respectively. It is observed that the calibration curves reveal a linear response. The calibration was prepared for both MW-LIBS and LIBS. The slope of the calibration curve using MW-LIBS was higher than that of LIBS. The reason for this has already been described in our previous paper.[26] The LoD was calculated using the 3-sigma method.[39] From the calibration curve, a 106 ± 6 μg g^{-1} LoD was obtained for fluorine using MW-LIBS where with LIBS it was 406.54 μg g^{-1} only. The relatively improved LoD with MW-LIBS was due to the enhanced signal of MW-LIBS. It was estimated that the enhanced CaF signal was 8 times better using MW-LIBS. This detection limit was not the best in terms of value because Alvarez *et al.*[14] reported a 0.49 μg g^{-1} detection limit. However, in terms of laser energy used, we have achieved 106 ± 6 μg g^{-1} at 10 mJ laser energy whereas Alvarez *et al.*[14] reported 0.49 μg g^{-1} at 100 mJ laser energy. A better enhancement was found for the CaBr signal, evaluated to be 15-fold. The LoD of 0.2 ± 0.04% was estimated for bromine using MW-LIBS which was 4 times higher than when utilising LIBS. With LIBS the LoD was 0.8 ± 0.2%. Using molecular emission, this study is the first to report the Br detection limit.

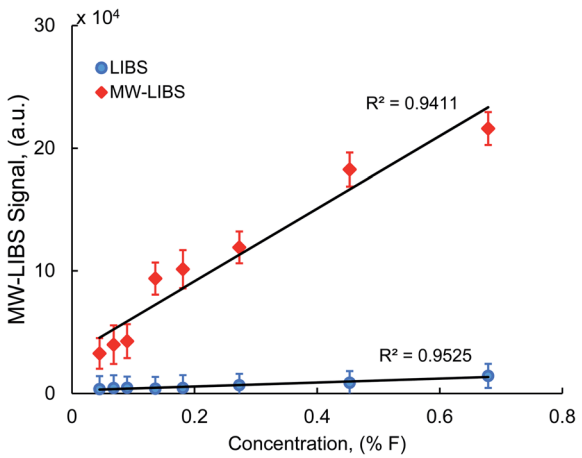

Fig. 6 Calibration curve of F using CaF molecular emission at a 10 mJ laser energy, 600 W microwave power, 400 ns gate-delay, 300 μs gate-width and accumulation of 100 shots.

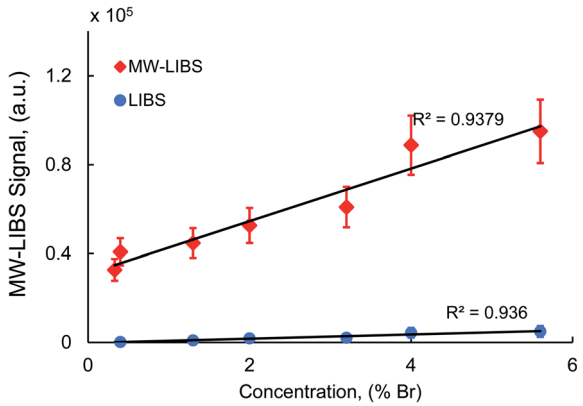

Fig. 7 Calibration curve of Br using CaBr molecular emission at a 15 mJ laser energy, 750 W microwave power, 400 ns gate-delay, 300 μs gate-width and accumulation of 100 shots.

4. Conclusion

The main goal of this work was to quantify and accurately detect fluorine and bromine. The MW-LIBS technique was employed *via* molecular emission bands on samples with different F and Br contents. Several possible emission spectra of CaF and CaBr were tested in the visible region. Optimum experimental conditions were demonstrated using CaF emission bands at 603.3 nm and 605 nm. In addition, plasma parameters have been analysed at different laser energies at constant microwave power coupling to optimise the laser energy. Using MW-LIBS, at 400 ns gate-delay, LoD values of 106 ± 6 μg g^{-1} and 0.2 ± 0.04% were calculated for F and Br, respectively. The LoD was calculated using LIBS for F and Br and found to be 406.54 μg g^{-1} and 0.8 ± 0.2%, showing that there was a quadruple improvement in the LoD with MW-LIBS. The LoD was obtained using a linear calibration curve of samples containing an increasing order of F and Br concentrations in the samples. This study also reports a quadruple improvement in the detection limit of Br reported in the literature.

Conflicts of interest

There is no conflict of interest.

References

1 S. United and C. Clement International, *Toxicological profile for fluorides, hydrogen fluoride, and fluorine*, U.S. Dept. of Health and Human Services, Public Health Service, Agency for Toxic Substances and Disease Registry, Atlanta, Ga., 1993.

2 C. Alvarez-Llamas, J. Pisonero and N. Bordel, *Spectrochim. Acta, Part B*, 2016, **123**, 157–162.
3 P. Pořízka, S. Kaski, A. Hrdlička, P. Modlitbová, L. Sládková, H. Häkkänen, D. Prochazka, J. Novotný, P. Gadas, L. Čelko, K. Novotný and J. Kaiser, *J. Anal. At. Spectrom.*, 2017, **32**, 1966–1974.
4 M. Gaft, L. Nagli, N. Eliezer, Y. Groisman and O. Forni, *Spectrochim. Acta, Part B*, 2014, **98**, 39–47.
5 C. González de Vega, C. Álvarez Llamas, N. Bordel, R. Pereiro and A. Sanz-Medel, *Anal. Chim. Acta*, 2015, **877**, 33–40.
6 I. Rae, *Global Environ.*, 2014, 7.
7 M. Gaft, L. Nagli, Y. Raichlin, F. Pelascini, G. Panzer and V. M. Ros, *Spectrochim. Acta, Part B*, 2019, **157**, 47–52.
8 R. Landau, *Corrosion*, 1952, **8**, 283–288.
9 A. Macías and M. L. Escudero, *Corros. Sci.*, 1994, **36**, 2169–2180.
10 Y. Wang, S. Zhang, X. Ji, P. Wang and W. Li, *Int. J. Electrochem. Sci.*, 2018, 4891–4900, DOI: 10.20964/2018.05.33.
11 A. Stájer, K. Ungvári, I. K. Pelsőczi, H. Polyánka, A. Oszkó, E. Mihalik, Z. Rakonczay, M. Radnai, L. Kemény, A. Fazekas and K. Turzó, *J. Biomed. Mater. Res., Part A*, 2008, **87**, 450–458.
12 J. Serrano, J. Moros and J. J. Laserna, *Anal. Chem.*, 2015, **87**, 2794–2801.
13 J. Viljanen, Z. Sun and Z. T. Alwahabi, *Spectrochim. Acta, Part B*, 2016, **118**, 29–36.
14 C. Alvarez-Llamas, J. Pisonero and N. Bordel, *J. Anal. At. Spectrom.*, 2017, **32**, 162–166.
15 G. Asimellis, S. Hamilton, A. Giannoudakos and M. Kompitsas, *Spectrochim. Acta, Part B*, 2005, **60**, 1132–1139.
16 C. D. Quarles, J. J. Gonzalez, L. J. East, J. H. Yoo, M. Morey and R. E. Russo, *J. Anal. At. Spectrom.*, 2014, **29**, 1238–1242.
17 T. Kratochvíl, M. Pouzar, K. Novotný, V. Havránek, T. Černohorský and M. Zvolská, *Spectrochim. Acta, Part B*, 2013, **88**, 26–31.
18 M. Wang, M. Zhao, S. Ye, M. Zhu, R. Yi, L. Liu and J. Qu, *J. Anal. At. Spectrom.*, 2018, **33**, 713–719.
19 L. Radziemski, D. A. Cremers, K. Benelli, C. Khoo and R. D. Harris, *Spectrochim. Acta, Part B*, 2005, **60**, 237–248.
20 S. Barbier, S. Perrier, P. Freyermuth, D. Perrin, B. Gallard and N. Gilon, *Spectrochim. Acta, Part B*, 2013, **88**, 167–173.
21 Y. Ikeda and R. Tsuruoka, *Appl. Opt.*, 2012, **51**, B183–B191.
22 D. E. Anderson, B. L. Ehlmann, O. Forni, S. M. Clegg, A. Cousin, N. H. Thomas, J. Lasue, D. M. Delapp, R. E. McInroy, O. Gasnault, M. D. Dyar, S. Schroder, S. Maurice and R. C. Wiens, *J. Geophys. Res.: Planets*, 2017, **122**, 744–770.
23 O. Forni, M. Gaft, M. J. Toplis, S. M. Clegg, S. Maurice, R. C. Wiens, N. Mangold, O. Gasnault, V. Sautter, S. Le Mouélic, P.-Y. Meslin, M. Nachon, R. E. McInroy, A. M. Ollila, A. Cousin, J. C. Bridges, N. L. Lanza and M. D. Dyar, *Geophys. Res. Lett.*, 2015, **42**, 1020–1028.
24 A. Khumaeni, K. Akaoka, M. Miyabe and I. Wakaida, *Front. Phys.*, 2016, **11**, 114209.
25 Y. Tang, J. Li, Z. Hao, S. Tang, Z. Zhu, L. Guo, X. Li, X. Zeng, J. Duan and Y. Lu, *Opt. Express*, 2018, **26**, 12121–12130.
26 M. A. Wakil and Z. T. Alwahabi, *J. Anal. At. Spectrom.*, 2019, **34**, 1892–1899.
27 M. Bahreini, B. Ashrafkhani and S. H. Tavassoli, *Appl. Phys. B: Lasers Opt.*, 2014, **114**, 439–447.
28 S. J. Chen, A. Iqbal, M. Wall, C. Fumeaux and Z. T. Alwahabi, *J. Anal. At. Spectrom.*, 2017, **32**, 1508–1518.
29 J. Zalach and S. Franke, *J. Appl. Phys.*, 2013, **113**, 043303.
30 S. Harilal, C. Bindhu, R. Issac, V. P. N. Nampoori and C. Vallabhan, *J. Appl. Phys.*, 1997, **82**, 2140–2146.
31 M. Dimitrijevic and S. Sahal-Brechot, *Serb. Astron. J.*, 2000, **161**, 39–88.
32 R. W. P. McWhirter, *Plasma Diagnostic Techniques*, ed. R. H. Huddlestone and S. L. Leonard, Academic Press, New York, 1965, pp. 201–264.
33 V. N. Rai and S. N. Thakur, in *Laser-Induced Breakdown Spectroscopy*, ed. J. P. Singh and S. N. Thakur, Elsevier, Amsterdam, 2007, pp. 83–111.
34 J. Reader, C. H. Corliss, W. L. Wiese and G. A. Martin, *Wavelengths and transition probabilities for atoms and atomic ions : part I. wavelengths - part II. transition probabilities*, National Bureau of Standards, NSRDS, NIST Research Library, Fedlink, Americana, 1980.
35 C. Bahrini, S. Douin, J. Rostas and G. Taieb, *Chem. Phys. Lett.*, 2006, **432**, 1–5.
36 D. Vogt, K. Rammelkamp, S. Schröder and H.-W. Hübers, *presented in part at the LPSC 2017*, The Woodlands, USA, 2017.
37 Y. A. Liu, M. Baudelet and M. Richardson, *J. Anal. At. Spectrom.*, 2010, **25**, 1316–1323.
38 A. A. Al Shuaili, A. M. Al Hadhrami, M. A. Wakil and Z. T. Alwahabi, *Spectrochim. Acta, Part B*, 2019, **159**, 105666.
39 S. Rosenwasser, G. Asimellis, B. Bromley, R. Hazlett, J. Martin, T. Pearce and A. Zigler, *Spectrochim. Acta, Part B*, 2001, **56**, 707–714.

